Eur. Phys. J. C 48, 125–133 (2006)
Digital Object Identifier (DOI) 10.1140/epjc/s2006-02611-x

THE EUROPEAN PHYSICAL JOURNAL C

Nuclear effects in deep inelastic scattering of charged-current neutrino off nuclear target

C.-G. Duan[1,2,3,4,a], G.-L. Li[1,3], P.-N. Shen[3,1,5,6]

[1] Institute of High Energy Physics, CAS, P.O. Box 918(4), Beijing 100049, China
[2] Department of Physics, Hebei Normal University, Shijiazhuang, 050016, China
[3] CCAST(World Laboratory), P.O. Box 8730, Beijing 100080, China
[4] Graduate School of the Chinese Academy of Sciences, Beijing 100049, China
[5] Institute of Theoretical Physics, Chinese Academy of Sciences, P.O. Box 2735, Beijing 100080, China
[6] Center of Theoretical Nuclear Physics, National Laboratory of Heavy Ion Accelerator, Lanzhou 730000, China

Received: 18 April 2006 / Revised version: 30 May 2006 /
Published online: 26 July 2006 –

Abstract. The nuclear effects in the neutrino–nucleus charged-current inelastic scattering process is studied by analyzing the CCFR and NuTeV data. The structure functions $F_2(x, Q^2)$ and $xF_3(x, Q^2)$ as well as differential cross sections are calculated by using CTEQ parton distribution functions and the EKRS and HKN nuclear parton distribution functions, and these are compared with the CCFR and NuTeV data. It is found that the corrections of the nuclear effect to the differential cross section for the charged-current antineutrino scattering on the nucleus are negligible, the EMC effect exists in the neutrino structure function $F_2(x, Q^2)$ in the large x region, the shadowing and anti-shadowing effect occur in the distribution functions of valence quarks in the small and medium x region, respectively. It is also found that shadowing effects on $F_2(x, Q^2)$ in the small x region in the neutrino–nucleus and the charged-lepton–nucleus deep inelastic scattering processes are different. It is clear that the neutrino–nucleus deep inelastic scattering data should further be employed in restricting the nuclear parton distributions.

PACS. 13.15.+g; 24.85.+p; 25.30.-c

1 Introduction

In the past three decades, the quark and gluon distributions in hadrons and nuclei have been one of the most active frontiers in nuclear physics and particle physics. The nuclear parton distribution directly affects the interpretation of the data collected from the nuclear reactions at high energies, for example the nucleus–nucleus and the proton–nucleus interactions at RHIC [1] and LHC [2]. Considering the nuclear effect causing modifications on the parton distribution function should be an essential step for understanding the suppression of J/ψ production which might be a signal of the quark–gluon plasma (QGP) in the relativistic heavy ion collision. Precisely modified nuclear parton distributions would especially be important in determining the electro-weak parameters, neutrino masses and mixing angles in neutrino physics.

In 1982, the European Muon Collaboration (EMC) reported that the measured ratio of nuclear structure functions for heavy (iron) and light (deuteron) nuclei in the processes of the deep inelastic scattering (DIS) of muons off the nucleus [3] is significantly different from the theoretically predicted value [4]. That was the first clear evidence for the nuclear effect in the nuclear structure functions, and it later was called the EMC effect. In fact, the EMC effect states that, in the parton point of view, quark distributions in a bound nucleon are different from those in a free nucleon. The discovery of the EMC effect triggered further studies on the sizable nuclear effect through the DIS of muons and electrons the off nucleus [5–8]. The abundant charged-lepton DIS data showed that there are four types of nuclear effects: the shadowing effect, the anti-shadowing effect, the EMC effect and the Fermi motion effect, appearing in the regions of $x < 0.1$, $0.1 < x < 0.3$, $0.3 < x < 0.7$ and $x > 0.7$, where x denotes the Bjorken variable, respectively.

Like the charged-lepton DIS, deep inelastic neutrino scattering is also an important process for investigating the structures of hadrons and nuclei. In this process, the structure functions $F_2(x, Q^2)$ and the parity-violating structure function $xF_3(x, Q^2)$ can simultaneously be measured. In 1984, the Big European Bubble Chamber Collaboration (BEBC) published the antineutrino–neon/deuterium DIS data in the kinematic region of $0 < x < 0.7$ and $0.25 < Q^2 < 26\,\mathrm{GeV}^2$ [9]. Their measured differential cross section ratio in the high Q^2 and

[a] e-mail: duancg@mail.hebtu.edu.cn

$0.3 < x < 0.6$ region [9] is compatible with the muon and electron the scattering data from EMC and SLAC. In the same year, CERN–Dortmund–Heidelberg–Saclay Collaboration (CDHS) measured events originating in a tank of liquid hydrogen and in the iron of detectors in the 400 GeV neutrino wide-band beam of the CERN Super Proton Synchrotron (SPS) [10]. Comparing the measured total cross sections, the differential cross sections and structure functions for hydrogen with those for iron, no significant difference between the structure functions for protons and iron was observed. One year later, the E545 Collaboration at Fermilab [11] measured the cross sections in deep inelastic neutrino scattering on neon or deuterium once more. Unfortunately, they were not able to give a definite conclusion due to substantial statistical uncertainties. In 1987, the WA25 and WA29 Collaborations studied the nucleon structure functions taken from the neutrino and antineutrino experiments for neon and deuterium [12]. The combined neutrino and antineutrino differential cross section data also showed that the cross section ratios between the heavy targets and deuterium decrease when x increases from 0.2 to 0.6, which is again the EMC effect. In fact, many neutrino DIS experiments were carried out with their own primary physical goals, for instance the structure of the proton, the mixing angles of the electro-weak interaction etc., but none of them can individually confirm the EMC effect.

In the early 1960's, Adler [13] proved that in the $Q^2 \to 0$ limit, the structure function $F_2(x, Q^2)$ obtained from the charged-lepton DIS process should go to zero, but $F_2(x, Q^2)$ from the neutrino DIS process should approach a positive constant. This discrepancy is caused by the partial conservation of axial currents (PCAC) in the weak interaction. With the aid of Adler's theorem, Bell [14] predicted that under certain kinematical conditions, the inelastic neutrino–nucleus interaction should demonstrate the shadowing effect. Later, the WA59 Collaboration [15] compared the kinematical distributions of neutrino and antineutrino events in the neon and deuterium target experiments under similar experimental conditions. Their results showed that the neutrino and antineutrino charged cross sections per nucleon in neon are relatively smaller than those in deuterium at low Q^2. This is the first experimental evidence of the shadowing effect in neutrino interactions, and it is consistent with the PCAC prediction.

The structure functions in the cross section formulas of DIS are merely related to the quark densities. An essential point of the quark–parton model is the universality of the quark and gluon densities, no matter if they are measured in the electromagnetic current interaction or the neutrino charge current or the neutrino neutral current interactions. Therefore, the only discrepancy in the neutrino and the charged-lepton DIS is the shadowing effect; the other nuclear effects in the two cases should be consistent.

Although there is no individual neutrino experiment on the EMC effect, the differential cross sections and structure functions have been measured in neutrino–nucleus experiments in CCFR [16–18] and NuTeV [19] at Fermilab, and in CDHSW [20] and CHORUS [21] at CERN. These experimental data would help us to understand the nuclear effects in the neutrino–nucleus interaction further.

The global analysis of nuclear parton distribution functions were carried out by Eskola et al. [22], Hirai et al. [23, 24] and de Florian and Sassot [25], respectively. In those analyses, the leading-order (LO) Dokshitzer–Gribov–Lipatov–Altarelli–Parisi (DGLAP) evolution was done by the first two groups, while the next-to-leading-order (NLO) evolution was performed by the third group. In 1999, Eskola, Kolhinen, Ruuskanen and Salgado (EKRS) suggested a set of nuclear parton distributions by using the F_2^A/F_2^D data in deep inelastic lA collisions and the nuclear Drell–Yan dilepton cross sections measured in pA collisions. The covered kinematical ranges were $10^{-6} \leq x \leq 1$ and $2.25\,\mathrm{GeV}^2 \leq Q^2 \leq 10^4\,\mathrm{GeV}^2$ for the nuclear targets from deuteron to heavy ones. Their results agree very well with the relevant EMC data and the E772 data at Fermilab [26]. In 2001, Hirai, Kumano and Miyama (HKM) [23] proposed quadratic and cubic types of nuclear parton distributions whose parameters were determined by a χ^2 global fit to the available experimental data, except those from the proton–nucleus Drell–Yan process. The covered kinematical ranges were $10^{-9} \leq x \leq 1$ and $1\,\mathrm{GeV}^2 \leq Q^2 \leq 10^5\,\mathrm{GeV}^2$ for deuteron and heavy nuclear targets. Their results reasonably explained the measured data of F_2. In 2004, Hirai, Kumano and Nagai (HKN) [24] re-analyzed the measured ratios of the nuclear structure functions $F_2^A/F_2^{A'}$ and the ratios of the Drell–Yan cross sections between different nuclei for obtaining another parton distribution function in nuclei. By employing the Drell–Yan data [26, 27], as well as the HERMES data [28], HKN determined the sea quark modification in the range of $0.02 < x_2 < 0.2$. It should be mentioned that up to now no neutrino–nucleus DIS data have been included in the analysis.

In this work, by means of the global LO DGLAP analyses of nuclear parton distribution functions, the differential cross sections and the structure functions $F_2(x, Q^2)$ and $xF_3(x, Q^2)$ in the neutrino–nucleus and antineutrino–nucleus charged-current DIS are calculated and compared with the relevant data from Fermilab. It is found that in the medium and high x regions, the anti-shadowing and the EMC effects in the structure functions are the same, but the nuclear corrections in the differential cross sections of antineutrino charged-current DIS are distinguishable. In Sect. 2, a brief formulism for the differential cross section and the structure function in the charged-current neutrino DIS is presented. The result and a discussion are given in Sect. 3, and the summary is given in Sect. 4.

2 Brief formalism for differential cross section and structure functions in charged-current neutrino DIS

In the lab frame, inclusive neutrino (antineutrino)–nucleon DIS [29–32] can be described by three kinematic variables: the squared momentum transfer Q^2, the incoming neutrino (antineutrino) energy E, and the inelasticity variable

y representing the fractional energy transferred to the final hadronic system. Q^2 can be expressed in terms of the fraction x of the bound nucleon momentum,

$$Q^2 = 2xyM_N E, \tag{1}$$

where M_N is the nucleon mass. If the parton mass is neglected, both x and y range from 0 to 1.

In the single-W exchange approximation, the differential cross sections for the charged-current neutrino (antineutrino)–nucleus process in the very small final lepton mass limit can be written as

$$\begin{aligned}\frac{\mathrm{d}^2\sigma^{\nu,\bar{\nu}}}{\mathrm{d}x\mathrm{d}y} = \frac{G_\mathrm{F}^2 E M_N}{\pi\left(1+Q^2/M_W^2\right)}\Bigg[&\frac{y^2}{2}2xF_1(x,Q^2)\\ &+\left(1-y-\frac{M_N xy}{2E}\right)F_2(x,Q^2)\\ &\pm y\left(1-\frac{y}{2}\right)xF_3(x,Q^2)\Bigg],\end{aligned} \tag{2}$$

where G_F is the weak Fermi coupling constant, M_W denotes the mass of the W boson, and the + and − signs correspond to ν and $\bar{\nu}$ scattering, respectively. In this equation, there are three structure functions: $2xF_1(x,Q^2)$, $F_2(x,Q^2)$ and $xF_3(x,Q^2)$. The first two structure functions are analogous to those for charged-lepton DIS. The third structure function $xF_3(x,Q^2)$ appears only in the weak interaction due to the parity-violation term in the product of the leptonic and hadronic tensors.

In order to account for the threshold correction of the heavy quark production, a so-called slow re-scaling method is employed [33]. Then the structure function should be scaled by ξ_S, rather than x,

$$\xi_\mathrm{S} = x\left(1+\frac{m_k^2}{Q^2}\right), \tag{3}$$

where m_k is the heavy quark mass with flavor k. The target mass effect is further taken into account by evaluating quark distributions at the Nachtmann variable ξ_N [34], rather than the Bjorken variable x:

$$\xi_\mathrm{N} = \frac{2x}{1+\sqrt{1+4M_N^2x^2/Q^2}}. \tag{4}$$

At high Q^2 ($Q^2 \gg M_N^2$), ξ_N is equivalent to x. When the target mass and heavy quark mass effects are simultaneously taken into account, the Bjorken scaling variable x should be replaced by

$$\xi_k = 2x\frac{1+\frac{m_k^2}{Q^2}}{1+\sqrt{1+\frac{4M_N^2x^2}{Q^2}\left(1+\frac{m_k^2}{Q^2}\right)}}. \tag{5}$$

In the quark–parton model, the structure functions are determined in terms of the quark distribution functions $u(x,Q^2), d(x,Q^2), s(x,Q^2), c(x,Q^2)$ and the gluon distribution function $g(x,Q^2)$, which satisfy QCD Q^2-evolution equations. Using the above mentioned ingredients, the structure function $F_1(x,Q^2)$ in the neutrino charged-current reaction can be written as

$$\begin{aligned}&F_1^{W^+p}(x,Q^2)\\ &= d\left(\xi_\mathrm{N},Q^2\right)|V_{ud}|^2 + d\left(\xi_c,Q^2\right)|V_{cd}|^2\theta(\xi_{\mathrm{N}c}-\xi_\mathrm{N})\\ &\quad+\bar{u}\left(\xi_\mathrm{N},Q^2\right)\left(|V_{ud}|^2+|V_{us}|^2\right)\\ &\quad+\bar{u}\left(\xi_b,Q^2\right)|V_{ub}|^2\theta\left(\xi_{\mathrm{N}b}-\xi_\mathrm{N}\right)\\ &\quad+s\left(\xi_\mathrm{N},Q^2\right)|V_{us}|^2 + s\left(\xi_c,Q^2\right)|V_{cs}|^2\theta(\xi_{\mathrm{N}c}-\xi_\mathrm{N})\\ &\quad+\bar{c}\left(\xi_\mathrm{N},Q^2\right)\left(|V_{cd}|^2+|V_{cs}|^2\right)\\ &\quad+\bar{c}\left(\xi_b,Q^2\right)|V_{cb}|^2\theta\left(\xi_{\mathrm{N}b}-\xi_\mathrm{N}\right),\end{aligned} \tag{6}$$

because the virtual W^+ coupled to the quarks with negative charge. Similarly, the structure function $F_1(x,Q^2)$ in the antineutrino charge-changing reaction can be expressed as

$$\begin{aligned}&F_1^{W^-p}(x,Q^2)\\ &= u\left(\xi_\mathrm{N},Q^2\right)\left(|V_{ud}|^2+|V_{us}|^2\right)\\ &\quad+u\left(\xi_b,Q^2\right)|V_{ub}|^2\theta(\xi_{\mathrm{N}b}-\xi_\mathrm{N})\\ &\quad+\bar{d}\left(\xi_\mathrm{N},Q^2\right)|V_{ud}|^2 + \bar{d}\left(\xi_c,Q^2\right)|V_{cd}|^2\theta(\xi_{\mathrm{N}c}-\xi_\mathrm{N})\\ &\quad+\bar{s}\left(\xi_\mathrm{N},Q^2\right)|V_{us}|^2 + \bar{s}\left(\xi_c,Q^2\right)|V_{cs}|^2\theta\left(\xi_{\mathrm{N}c}-\xi_\mathrm{N}\right)\\ &\quad+c\left(\xi_\mathrm{N},Q^2\right)\left(|V_{cd}|^2+|V_{cs}|^2\right)\\ &\quad+c\left(\xi_b,Q^2\right)|V_{cb}|^2\theta(\xi_{\mathrm{N}b}-\xi_\mathrm{N}),\end{aligned} \tag{7}$$

because of the virtual W^- coupling to the quarks with positive charge. In these two equations, the quantities V_{ij} are the Cabibbo–Kobayashi–Maskawa (CKM) quark mixing matrix elements [35], $\theta(\xi_{\mathrm{N}c}-\xi_\mathrm{N})$ and $\theta(\xi_{\mathrm{N}b}-\xi_\mathrm{N})$ are step functions. The quantity $\xi_{\mathrm{N}k}$ can be defined as

$$\xi_{\mathrm{N}k} = \frac{Q^2}{Q^2+(M_X^{\min})^2-M_N^2}, \tag{8}$$

where $M_X^{\min}$ is the minimum mass of the final hadron system for the light quark transition to the heavy quark k.

The structure functions $F_2^{W^\pm p}(x,Q^2)$ and $F_3^{W^\pm p}(x,Q^2)$ can be obtained from (6) and (7) by making the replacements indicated in the curly brackets:

$$\begin{aligned}F_2^{W^\pm p}(x,Q^2) = F_1^{W^\pm p}\big\{&q\left(\xi_\mathrm{N},Q^2\right)\to 2xq\left(\xi_\mathrm{N},Q^2\right),\\ &q\left(\xi_k,Q^2\right)\to 2\xi_k q\left(\xi_k,Q^2\right)\big\},\end{aligned} \tag{9}$$

$$F_3^{W^\pm p}(x,Q^2) = 2F_1^{W^\pm p}\left\{\bar{q}\left(\xi_\mathrm{N},Q^2\right)\to -\bar{q}\left(\xi_\mathrm{N},Q^2\right)\right\}. \tag{10}$$

Assuming isospin symmetry, the corresponding neutron structure functions can be obtained from the proton ones by making the replacements $u(x,Q^2)\to d(x,Q^2)$ and $\bar{u}(x,Q^2)\to\bar{d}(x,Q^2)$.

In charged-lepton DIS, the structure function $F_2(x,Q^2)$ is related to the structure function $2xF_1(x,Q^2)$ by the well-known Callan–Gross relation [36]. But this relation is only valid if the virtual photon is completely transverse. In fact, it has been observed that the Callan–Gross relation is not accurately obeyed, and the violation can usually be written as

$$2xF_1(x,Q^2) = \frac{1+4M^2x^2/Q^2}{1+R(x,Q^2)}F_2(x,Q^2), \tag{11}$$

where $R(x,Q^2)$ is the ratio of the cross sections for the longitudinally polarized photon to the transversely polarized photon. An analogous relation should hold in neutrino DIS. The CHORUS [21] results on $R(x,Q^2)$ are in agreement with the more precisely measured values in charged-lepton scattering. By fitting the experimental data available, Whitlow et al. [37] gave an general expression:

$$R(x,Q^2)=\frac{0.0635}{\log(Q^2/0.04)}\theta(x,Q^2)+\frac{0.5747}{Q^2}-\frac{0.3534}{Q^4+0.09}, \tag{12}$$

where

$$\theta(x,Q^2)=1.0+\frac{12Q^2}{Q^2+1.0}\times\frac{0.125^2}{0.125^2+x^2}\,.$$

3 Results and discussion

The structure functions $F_2(x,Q^2)$ and $xF_3(x,Q^2)$ obtained from neutrino scattering experiments are usually extracted from the sum and the difference of the neutrino and the antineutrino y-dependent differential cross sections, respectively. The structure function $F_2(x,Q^2)$ can be expressed by the average of $F_2^{\nu A}(x,Q^2)$ and $F_2^{\bar{\nu}A}(x,Q^2)$, while the structure function $xF_3(x,Q^2)$ can be determined by $\frac{1}{2}(xF_3^{\nu A}(x,Q^2)+xF_3^{\bar{\nu}A}(x,Q^2))$. In order to compare with the experimental data, the expressions of $F_2(x,Q^2)$ and $xF_3(x,Q^2)$ are written as

$$F_2(x,Q^2)=\frac{1}{4}\left(F_2^{\nu p}(x,Q^2)+F_2^{\nu n}(x,Q^2)+F_2^{\bar{\nu}p}(x,Q^2)+F_2^{\bar{\nu}n}(x,Q^2)\right), \tag{13}$$

$$xF_3(x,Q^2)=\frac{1}{4}\left(xF_3^{\nu p}(x,Q^2)+xF_3^{\nu n}(x,Q^2)+xF_3^{\bar{\nu}p}(x,Q^2)+xF_3^{\bar{\nu}n}(x,Q^2)\right). \tag{14}$$

In our calculation, the values of the CKM matrix elements are taken from the global fit [38]. They are $V_{ud}=0.9739$, $V_{us}=0.221$, $V_{cd}=0.221$ and $V_{cs}=0.9730$. In the case of heavy quark production, only the structure functions related to the charm quark production are considered. The value of the charm quark mass is taken to be 1.31 GeV, which corresponds to the value obtained in the LO QCD analysis of dimuon events [39]. In terms of the CTEQ (coordinated theoretical experimental project on QCD) [40] parton distribution functions in proton and nuclear parton distribution functions from EKRS [22] and HKN [24] (called the EKRS fit and HKN fit, respectively, in the rest of the paper), the differential cross sections and the structure functions $F_2(x,Q^2)$ and $xF_3(x,Q^2)$ for charged-current neutrino and antineutrino scatterings from iron are calculated. The results are plotted in Figs. 1–5, where the solid and the dashed curves represent the results by using the EKRS and HKN nuclear parton distributions with nuclear effects, respectively, and the dotted curves denote the results by employing the CTEQ parton distributions without nuclear effects. The theoretical result of the structure function $F_2(x,Q^2)$ is compared with the NuTeV and CCFR experimental data in Fig. 1. In this figure, the experimental data are taken from [17] (open circle), [18] (solid circle) and [19] (open square), respectively. It seems that the CHORUS results [21] favor the CCFR data and the expected fact that the difference between the nuclear structure functions of lead and iron is small. Preliminary NuTeV data of $F_2(x,Q^2)$ [19] are generally consistent with the CCFR data in the low and medium x regions but become larger than the CCFR values when $x\geq 0.65$. This deviation should be confirmed in further experiments. It is shown that our results with nuclear effects agree excellently with the CCFR data in the region of $x\geq 0.45$, which clearly shows the EMC effect in the neutrino DIS. In the region of $0.18\leq x\leq 0.35$, the EKRS fit is in a good agreement with the experimental data, but the HKN fit apparently overestimates the values of the structure functions $F_2(x,Q^2)$. At $x=0.14$, the results from the EKRS and HKN fits show the same tendency with the experimental data. In the smaller x region, say $x=0.11$ or $x=0.09$, EKRS and HKN fits reasonably describe the experimental data. They also show the existence of anti-shadowing effect in the region of $0.09\leq x\leq 0.275$. In the very small x region, say $x<0.07$, the theoretical results apparently deviate from the experimental data with decreasing value of x, especially in the $x<0.0175$ region. It is well known that in the fixed target experiment the lower x value usually corresponds to a low Q^2 value. The low x and low Q^2 structure function $F_2(x,Q^2)$ from neutrino scattering experiments should not necessarily agree with those from the charged-lepton scattering experiment, because of the contributions from the PCAC of the weak interaction. The shadowing effect should be process-dependent, and it should be smaller in neutrino DIS than in charged-lepton DIS. So the difference of the structure function $F_2(x,Q^2)$ between the neutrino and the charged-lepton reactions should further be investigated in experimental and theoretical studies.

The behavior of the structure function $xF_3(x,Q^2)$ is presented in Fig. 2. In general, the CHORUS results [21] are in agreement with the CCFR and CDHSW [20] data. Preliminary NuTeV data are consistent with the CCFR data in the low and medium x regions, but show higher values at $x\geq 0.75$. Considering the nuclear effects, our calculated results reasonably agree with the experimental data in the region of $x\geq 0.45$, showing the same nuclear effect presented in the charged-lepton DIS. In the region of $0.18\leq x\leq 0.35$, the EKRS results agree with the experimental data, but the HKN results overestimate the structure function $xF_3(x,Q^2)$. In the smaller x region, say $x=0.11$ or $x=0.14$, EKRS and HKN fits cannot properly describe the experimental data. Moreover, in the $x\leq 0.09$ region, the HKN fit is consonant with the data, but the EKRS and CTEQ fits overestimate the values of the structure function $xF_3(x,Q^2)$. In charged-lepton DIS, it is not obvious whether the valence quark distribution indicates shadowing and anti-shadowing. Nevertheless, the neutrino DIS experimental data expose the shadowing and anti-shadowing effects in the nuclear valence quark distributions. In terms of the HKN nuclear parton distribution, one can well describe the shadowing effect, but still one over-

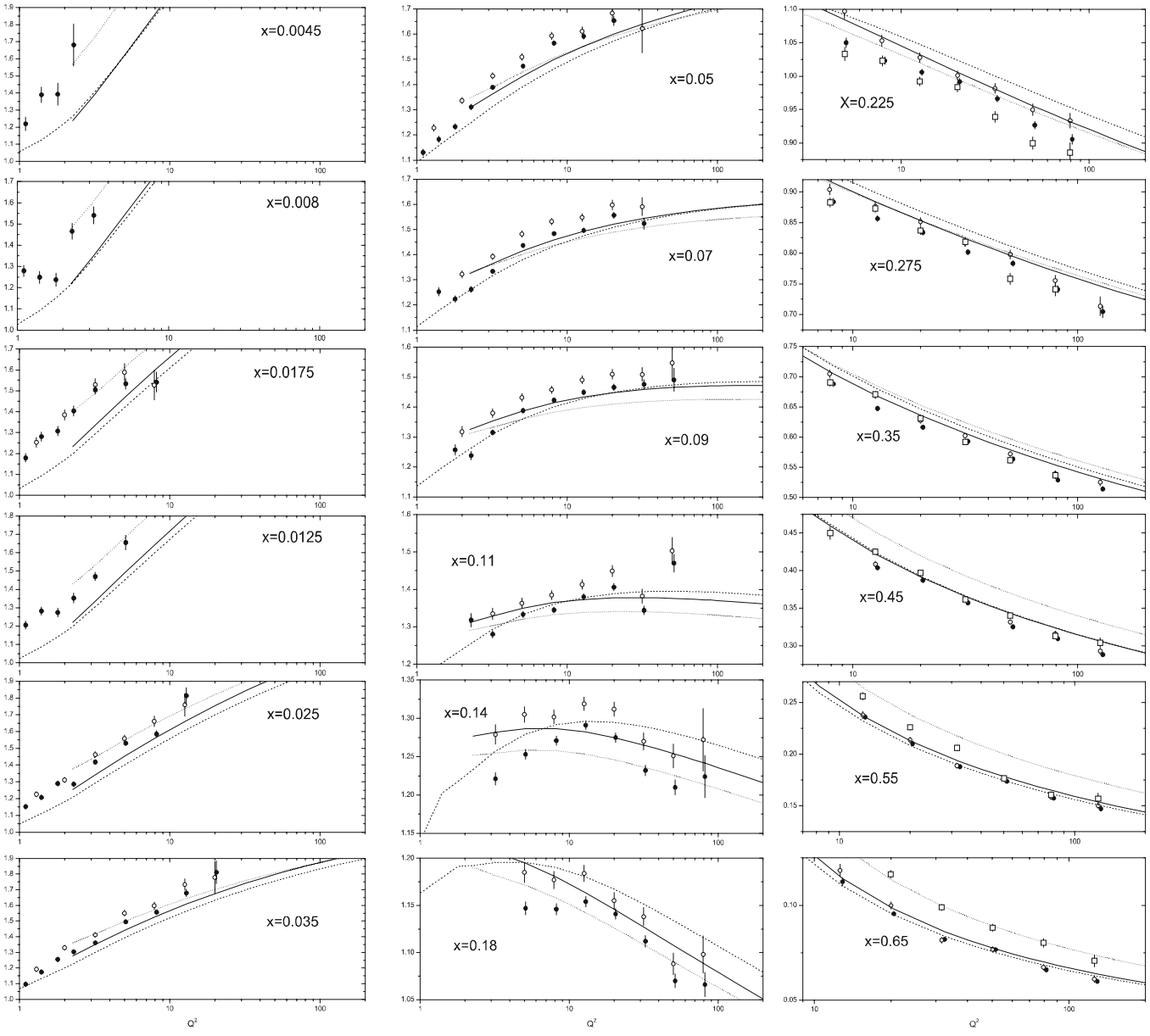

Fig. 1. The structure functions $F_2(x, Q^2)$ as a function of Q^2 at various Bjorken variables x. The experimental data are taken from [17] (*open circle*), [18] (*solid circle*) and [19] (*open square*), respectively. The *solid* and *dashed lines* are the results from the EKRS and HKN nuclear parton distributions with nuclear effects, respectively. The *dotted lines* are the results from the CTEQ parton distributions with no nuclear effects

estimates the anti-shadowing effect in the valence quark distribution.

The recombined experimental data and the structure function $xF_3(x, Q^2)$ with various Q^2 are shown in Fig. 3. From this figure, one sees that the HKN results consist excellently with the experimental data at the low and high x regions but overestimate the anti-shadowing effect of the valence quark in the bound nucleus in the medium x region with $Q^2 \leq 50.1\,\mathrm{GeV}^2$. Although the EKRS fit overestimates the values of the structure functions at smaller x in the $Q^2 \leq 12.6\,\mathrm{GeV}^2$ region, it is in very good agreement with the experimental data in the anti-shadowing and EMC effect regions with $Q^2 \geq 20.0\,\mathrm{GeV}^2$.

The differential cross sections as a function of y for charged-current neutrino (antineutrino) scattering on the iron nucleus are calculated in various x bins at $E = 85\,\mathrm{GeV}$. The results are plotted and compared with the experimental data in Fig. 4. It should be remarked that the NuTeV data [19] are reasonably in agreement with the CCFR and CDHSW data with the exception of the Bjorken variable region $x \geq 0.40$, where CCFR neutrino and antineutrino differential cross section data are unanimously below the NuTeV results. The comparison with the experimental data reveals that the nuclear corrections are negligible in the differential cross sections of charged-current antineutrino DIS, which is the same as that in [41], but the

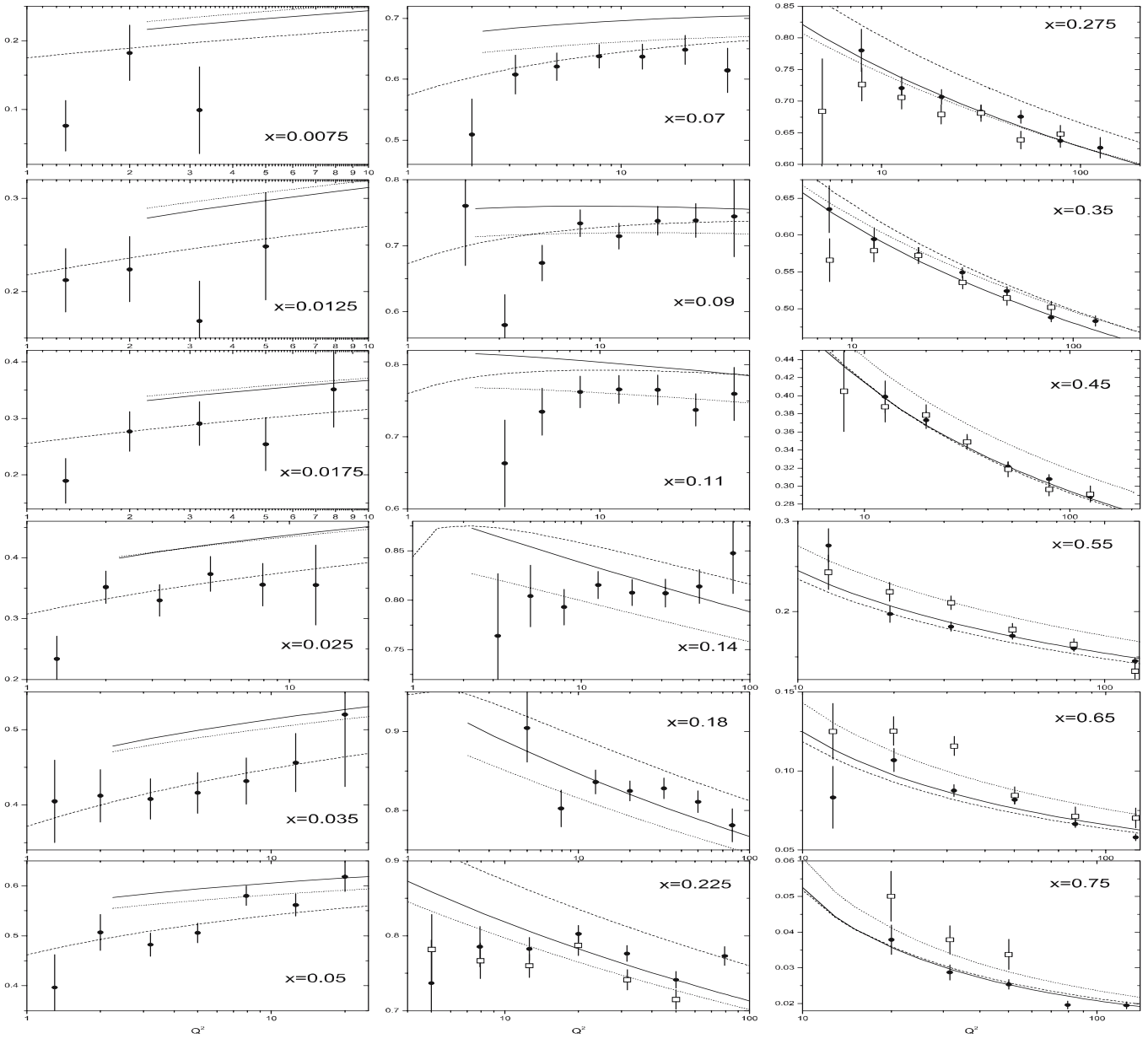

Fig. 2. The structure functions $xF_3(x, Q^2)$ as a function of Q^2 at various Bjorken variables x. The experimental data are taken from [17] (*solid circle*) and [19] (*open square*), respectively. The notation of the *curves* is the same as Fig. 1

neutrino–iron differential cross sections provide more information. It is seen that there are no nuclear effects in the region $x \leq 0.125$. The results from EKRS and CTEQ are in agreement with the experimental data, the HKN results greatly overestimate the neutrino–nucleus differential cross sections in the region of $0.175 \leq x \leq 0.35$. This is because the sign of the $xF_3(x, Q^2)$ term in the differential cross section of neutrino DIS is positive; the contributions from the valence quarks are dominant. For $x \geq 0.45$, it seems that these three fits overestimate the data a little bit.

Recently, Kulagin and Petti [42] (KP) and Qiu and Vitev [43] (QV) respectively predicted the nuclear corrections in the low x region. Because the HKN nuclear distribution can provide a good description for the structure function $xF_3(x, Q^2)$ at small x, we show the calculated ratios of $xF_3(Fe)$ to $xF_3(D)$ with different x and Q^2 values in Fig. 5 and tabulate them, as well as the KP and QV ones, in Table 1 for comparison. It is shown that the HKN fit presents suppressions of 7% and about 5% at $x = 0.0001$ and $x = 0.01$, respectively, while QV gave 15% at both $x = 0.0001$ and $x = 0.01$ with $Q^2 = 1.0\,\mathrm{GeV}^2$, and KP showed a larger nuclear suppression in the shadowing region.

In the global DGLAP analysis of nuclear effects, the abundant data are used. They are the ratios of the structure functions in electron and muon DIS and the ratios of the differential cross sections of the lepton pairs production in the nuclear Drell–Yan process for different nuclei, although the energy loss effect [44] might exist.

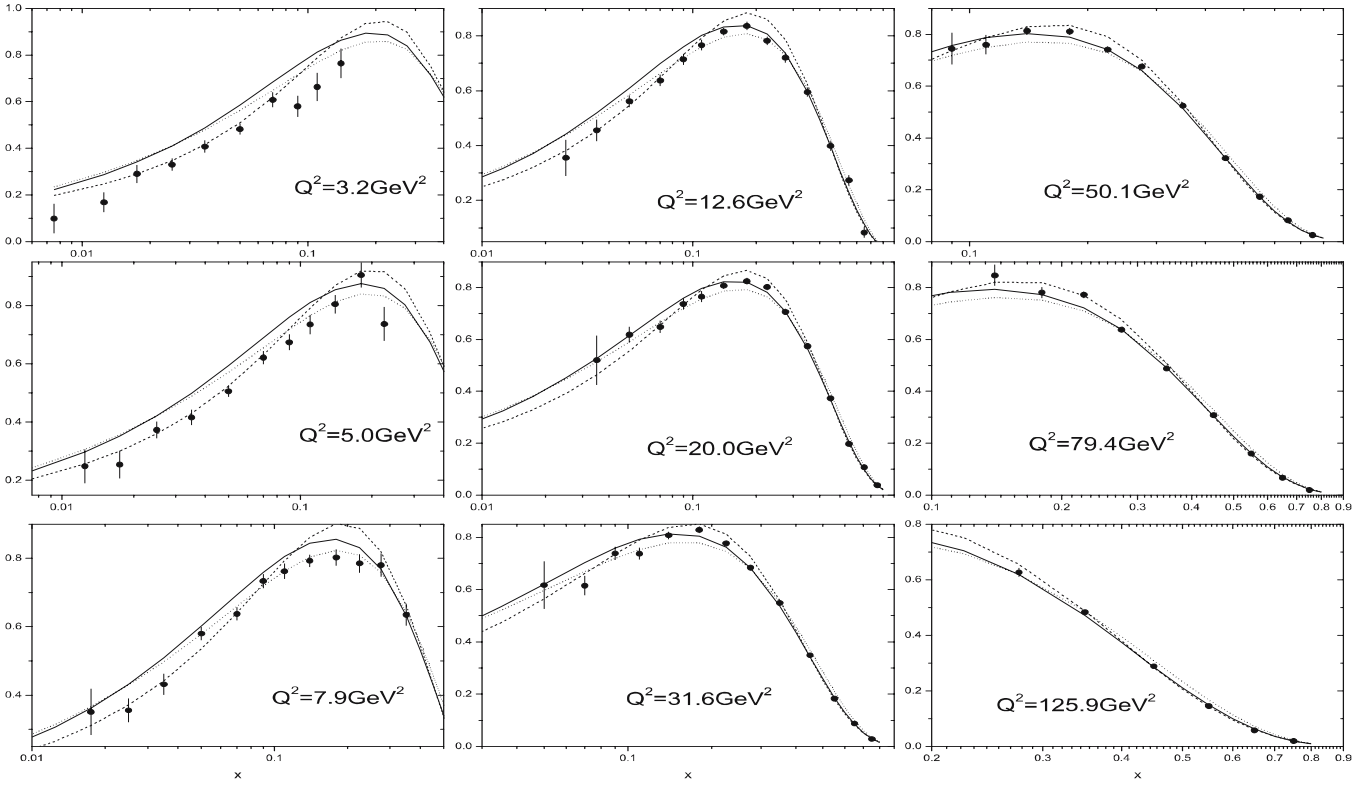

Fig. 3. The structure functions $xF_3(x, Q^2)$ as a function of the Bjorken variable x at various Q^2. The experimental data are taken from [17]. The notation of the *curves* is the same as Fig. 1

The data of nuclear structure functions in neutrino–nucleus DIS are so scarce that they have not been included in the current global fit for nuclear parton distributions. Consequently, it is difficult to determine nuclear valence quark distributions in the small x region and nuclear anti-quark distributions in the $x > 0.2$ region. In contrast, the nuclear valence quark distribution in the medium and large x regions can relatively well be determined. It is conventionally considered that the EMC effect and Fermi motion primarily occur in the scattering on valence quarks. The anti-shadowing occurring in the medium x region could be affected by either the sea or the valence quark contributions. The shadowing effect mainly comes from the scattering off a sea quark. The nuclear modifications for neutrino and charged-lepton scatterings should be expected to be identical without the lower x and lower Q^2 region due to the PCAC of the weak interaction. The experimental data of $xF_3(x, Q^2)$ present an obvious anti-shadowing effect of the valence quarks, which is absent in charged-lepton DIS.

Therefore, it would be plausible if the neutrino DIS experimental data can be included into the study of nuclear parton distributions. In fact, by means of the structure function $xF_3(x, Q^2)$ in neutrino DIS only, the nuclear modifications to the valence quark distribution can very precisely be determined in the medium and large x regions. With the structure functions $F_2(x, Q^2)$ from the neutrino and charged-leptons scatterings, the nuclear modifications to the sea quark distribution in the medium and large x regions would be pinned down. In addition, a detailed investigation of the nuclear correction in the lower x region is needed, because such a correction depends on whether the process is neutrino or charged-lepton DIS.

Table 1. The results in detail from HKN, QV and KP

	HKN			QV	KP	
$Q^2(\mathrm{GeV}^2)$	1.0	5.0	20.0	1.0	5.0	20.0
$x\ (10^{-4})$	0.929	0.931	0.933	0.85–0.88	0.76	0.88
$x\ (10^{-2})$	0.945	0.958	0.966	0.85–0.88	0.82	0.92

4 Concluding remarks

As a summary, a LO analysis of neutrino–nucleus DIS is performed. The structure functions $F_2(x, Q^2)$ and $xF_3(x, Q^2)$ and the differential cross sections are calculated and compared with the experimental data from CCFR and NuTeV by employing more appropriate EKRS and HKN nuclear parton distributions and CTEQ parton distributions without nuclear corrections. It is found that the nuclear corrections are negligible in the differential cross sections of the antineutrino charged-current DIS. The EMC effect does exist in the neutrino structure function $F_2(x, Q^2)$. Such an effect is as strong as that shown in the lepton structure function. Shadowing and anti-shadowing effects occur in $xF_3(x, Q^2)$ in the small and medium x re-

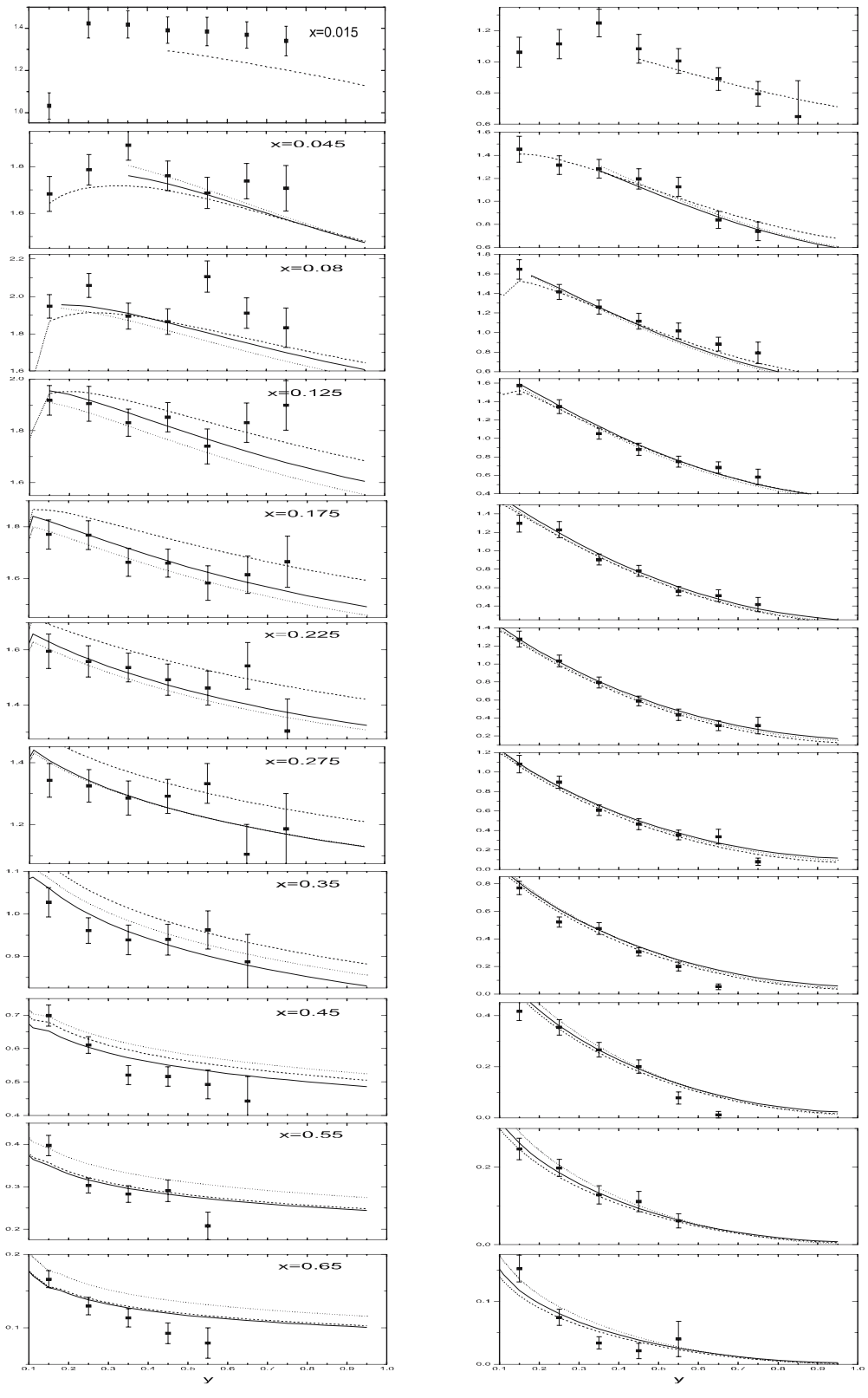

Fig. 4. The differential cross sections $\frac{1}{E}\frac{\mathrm{d}^2\sigma}{\mathrm{d}x\mathrm{d}y}$ (in 10^{-38} $\mathrm{cm}^2\,\mathrm{GeV}^{-1}$) as a function of y for neutrino (*left*) and antineutrino (*right*) at $E = 85\,\mathrm{GeV}$. The corresponding values of the Bjorken variable x are indicated in the figures on the *left*. The experimental data are taken from [16]. The notation of the *curves* is the same as Fig. 1

gion, respectively. It clearly demonstrates the shadowing and anti-shadowing effect of the valence quark distribution. Shadowing effects at small x in neutrino and lepton DIS are not exactly the same. This is due to the conservation of the vector current in lepton DIS and the PCAC of the weak interaction. The shadowing effect in neutrino DIS should be weaker than that in lepton DIS. Because of the process dependence of the shadowing effect, further investigations are required. It is necessary to measure the ratios of the structure functions $F_2(x, Q^2)$ (and $xF_3(x, Q^2)$) for

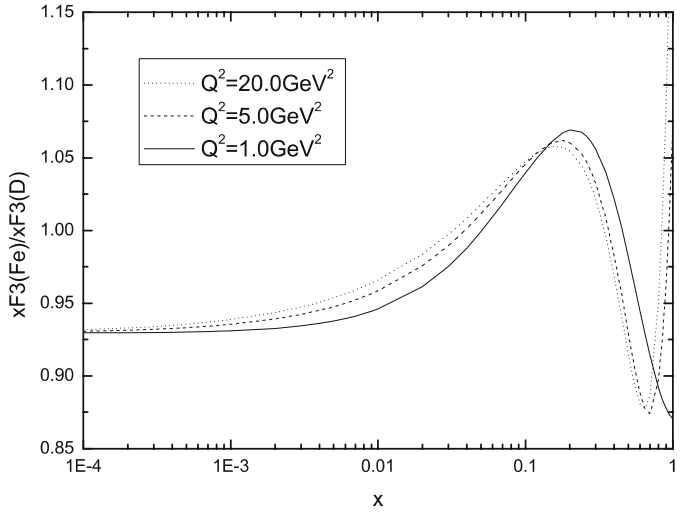

Fig. 5. The ratios of the structure functions $xF_3(x, Q^2)$ for iron and deuterium. The curves are drawn for $Q^2 = 1.0, 5.0, 20.0\ \mathrm{GeV}^2$ from the HKN nuclear parton distributions

various nuclei in neutrino DIS. The structure function $F_2(x, Q^2)$ is also very important to investigate the nuclear shadowing effect in the small x region by means of charged-lepton DIS, because the structure function ratios of the heavy nucleus to light nucleus are currently taking in lepton DIS experiments. The MINERv-A(Fermilab E938) [45] and neutrino-factory [46] projects will start in the near future. The study of the structure functions would deepen our knowledge of the shadowing effect on the valence quark and anti-quark distributions in the neutrino and the lepton DIS processes. Clarifying the shadowing effect will allow us to determine the nuclear modifications of parton distributions, to study the new state of matter in the heavy ion collision accurately, as well as to investigate the basic QCD and electro-weak parameters.

Acknowledgements. The authors thank D. Naples for the new NuTeV experimental data sent by e-mail. This work is partially supported by Natural Science Foundation of China (10475089, 10435080, 10575028), CAS Knowledge Innovation Project (KJCX2-SW-N02), Major State Basic Research Development Program (G20000774), Natural Science Foundation of Hebei Province(103143) and IHEP grant No.U529.

References

1. H.K. Ackermann et al., Nucl. Instrum. Method. A **499**, 624 (2003)
2. F. Carminati et al., J. Phys. G **30**, 1517 (2004)
3. J.J. Aubert et al., Phys. Lett. B **123**, (1983) 275
4. A. Bodek, J.L. Ritchie, Phys. Rev. D **23**, 1070 (1981); ibid **24**, 1400 (1981)
5. M. Arneodo, Phys. Rep. **240**, 301 (1994)
6. D.F. Geesaman, K. Saito, A.W. Thomas, Annu. Rev. Nucl. Part. Sci. **45**, 337 (1995)
7. G. Piller, W. Weise, Phys. Rep. **330**, 1 (2000)
8. P.R. Norton, Rep. Prog. Phys. **66**, 1253 (2003)
9. A.M. Cooper et al., Phys. Lett. B **141**, 133 (1984)
10. CDHS Collaboration, H. Abramowicz et al., Z. Phys. C **25**, 29 (1984)
11. J. Hanlon et al., Phys. Rev. D **32**, 2441 (1985)
12. J. Guy et al., Z. Phys. C **36**, 337 (1987)
13. S.L. Adler, Phys. Rev. B **135**, 963 (1964)
14. J.S. Bell, Phys. Rev. Lett. **13**, 57 (1964)
15. P.P. Allport et al., Phys. Lett. B **232**, 417 (1989)
16. CCFR Collaboration, U.K. Yang, Ph. D. Thesis, University of Rochester, (2001), UR-1583
17. CCFR Collaboration, W.G. Seligman et al., Phys. Rev. Lett. **79**, 1213 (1997)
18. CCFR Collaboration, B.T. Fleming et al., Phys. Rev. Lett. **86**, 5430 (2001)
19. NuTeV Collaboration, M. Tzanov et al., arXiv: hep-ex/0509010
20. CHORUS Collaboration, G. Onengut et al., Phys. Lett. B **623**, 65 (2006)
21. CDHSW Collaboration, J.P. Berge et al., Z. Phys. C **49**, 187 (1991)
22. K.J. Eskola, V.J. Kolinen, C.A. Salgado, Eur. Phys. J. C **9**, 61 (1999); K.J. Eskola, V.J. Kolinen, P.V. Ruuskanen, Nucl. Phys. B **535**, 351 (1998)
23. M. Hirai, S. Kumano, M. Miyama, Phys. Rev. D **64**, 034003 (2001)
24. M. Hirai, S. Kumano, T.H. Nagai, Phys. Rev. C **70**, 044905 (2004), arXiv: hep-ph/0404093
25. D. de Florian, R. Sassot, Phys. Rev. D **69**, 074028 (2004)
26. E772 Collaboration, D.M. Adle et al., Phys. Rev. Lett. **64**, 2479 (1990)
27. E866 Collaboration, M.A. Vasiliev et al., Phys. Rev. Lett. **83**, 2304 (1999)
28. HERMES Collaboration, A. Airapetian et. al., Phys. Lett., B **567**, 339 (2003)
29. S.R. Mishra, F. Sciulli, Annu. Rev. Nucl. Part. Sci. **39**, 269 (1989)
30. M. Diemoz, F. Ferroni, E. Longo, Phys. Rept. **130**, 293 (1986)
31. J.M. Conrad, M.H. Shaevitz, T. Bolton, Rev. Mod. Phys. **70**, 1341 (1998)
32. J.T. Londergan, A.W. Thomas, Prog. Part. Nucl. Phys. **41**, 49 (1998)
33. H. Georgi, H.D. Politzer, Phys. Rev. D **14**, 1829 (1976); R.M. Barnett, Physica D **14**, 70 (1976)
34. O. Nachtmann, Nucl. Phys. B **78**, 455 (1974)
35. M. Kobayashi, T. Maskawa, Prog. Theor. Phys. **49**, 652 (1973); N. Cabibbo, Phys. Rev. Lett. **10**, 531 (1963)
36. C.G. Callan, D.G. Gross, Phys. Rev. Lett. **22**, 156 (1969)
37. L.W. Whitlow et al., Phys. Lett. B **250**, 193 (1990)
38. Particle Data Group, Phys. Lett. B **592**, 1 (2004)
39. S.A. Rabinowitz et al., Phys. Rev. Lett. **70**, 134 (1993)
40. CTEQ Collaboration, H.L. Lai et al., Eur. Phys. J. C **5**, 461 (1998)
41. J.J. Yang et al., Phys. Lett. B **546**, 68 (2002)
42. S.A. Kulagin, H. Petti, arXiv: hep-ph/0412425
43. J.W. Qiu, I. Vitev, Phys. Lett. B **587**, 52 (2004), arXiv: hep-ph/0401062
44. C.G. Duan et al., Eur. Phys. J. C **39**, 179 (2005); ibid **29**, 557 (2003); C.G. Duan, H.M. Wang, G.L. Li, Chin. Phys. Lett. **19**, 485 (2002)
45. MINERvA(E938), arXiv: hep-ex/0405002
46. S. Kumano, arXiv: hep-ph/0310166